*Journal of Thermal Analysis, Vol. 48 (1997) 1229-1248*

# MODELLING SOLUTE SEGREGATION TO PARTIAL DISLOCATIONS FOR DSC EVALUATIONS

*A Varschavsky and E. Donoso*

Universidad de Chile, Facultad de Ciencias Físicas y Matemáticas, Instituto de Investigaciones y Ensayes de Materiales, Casilla 1420, Santiago, Chile

(Received July 26, 1996)

## Abstract

A general model is discussed for assessing the energy release due to the pinning of solute atoms to partial dislocations. The present approach discloses the influence of dislocation character distributions on the magnitude of this energy. In order to test its validity in αCu–Al alloys, differential scanning calorimetry (DSC) evaluations associated with the different peaks involved during linear heating were performed employing both cold worked and quenched materials. Dislocation densities were calculated from recrystallization traces. On the basis of this model it was concluded that the observed energy difference between the deformed and the quenched materials during the exothermic peak designated as Stage 2 corresponds to the pinning process. It was also concluded that nearly equal number of edge and screw dislocations are present in the dislocation configuration of deformed alloys. Nevertheless, it is proposed that dislocation-induced order might also occur as a consequence of enhanced solute concentration around the partials.

**Keywords**: αCu-Al alloys, dislocations, DSC, energetics, recrystallization, rolled, segregation, short-range-order

## Introduction

The flow stress of cold worked Cu solid solutions increases on annealing below the recrystallization temperature [1–4]. This strengthening effect, called anneal hardening [5–11], occurs in several Cu based solid solutions, of which Cu–Al is the one most studied. Three general trends characterizing the phenomenon in all alloy systems can be noted:

1) Strengthening that accompanies aging increases with increasing degree of prior cold work.

2) Strengthening due to aging increases with increasing substitutional element concentration.

3) Strengthening due to aging is a decreasing function of the plastic strain at which the strength is measured.

If property changes occurring during the annealing of cold worked alloys and the underlying processes are compared to the recovery of cold worked pure metals,

*0368–4466/97/ $ 5.00*


*John Wiley & Sons Limited*
*Chichester*

additional phenomena that may occur in alloys are found, viz. mutual interactions of different atomic species, short-range-order (SRO), and interactions of solute atoms with lattice defects. SRO in undeformed crystals does not lead to a significant increase in flow stress [10] which is comparable in magnitude to the effect of anneal hardening, although it may give rise to a marked yield drop [12, 13]. The interactions of solute atoms with lattice defects, however, may cause a considerable increase in flow stress due to vacancy and solute locking of dislocations, and solute segregation to stacking faults [14].

It is then important to test quantitatively the validity of the hypothesis that solute segregation to partial dislocations in the deformed condition gives rise to the predominant hardening mechanism. αCu–Al alloys were chosen since they may exhibit SRO along with solute segregation, thus illustrating an example where previous separation of both phenomena is necessary to recognize segregation effects. Differential scanning calorimetry was used as an effective experimental method in order to compute dislocation densities in the cold-roller alloys and also for assessing an energy balance compatible with the segregation processes occurring in addition to SRO formation characteristic of the quenched material.

Chiefly, the present work: (a) discloses a model that predicts the energy evolved by a solute segregation process to partial dislocations, which is appropriate to copper-based alloys due to their low stacking fault energy; (b) analyses the influence of certain dislocation character distributions on the magnitude of energy associated with the pinning effect; and (c) tests its validity for αCu–Al alloys in order to describe the events displayed by the DSC profiles.

## The segregation model

### *Binding energies*

In many alloy systems dislocations dissociate in partials due to the low value of stacking fault energy. Particularly in copper-based alloys, unit dislocations dissociate even at very low solute concentrations. For instance, in pure copper for a dissociated dislocation having stacking fault ribbon of width $w_s$ and Burgers vector $\mathbf{b}$, the value of $w_s/b$ is equal to five [15]. Such large value of $w_s$, allows to consider the pinning of each partial dislocation rather than the pair. Because of fcc structure crystallography, one or both partial dislocations will have a first order misfit with a substitutional solute atom. Thus, through the misfit interaction, a solute atom may interact with both dissociated edge and dissociated screw dislocations. Considering an undissociated dislocation with its line along vector $\mathbf{l}$, the edge component of $\mathbf{b}$ is $\mathbf{b}_e$ normal to $\mathbf{l}$, and the screw component is $\mathbf{b}_s$ parallel to $\mathbf{l}$, a solute atom located at $r$, $\theta$ interacts with the dislocation with interaction energies $\Delta H_a$ due to misfit and $\Delta H_m$ due to modulus interaction. Expressions for the $\Delta H$'s are given by Eshelby [16] and by Saxl [17], and in order to evaluate them the terms

$$e_a = \mathrm{d}\ln a/\mathrm{d}c$$

$$e_G = d\ln G/dc$$

$$e_k = d\ln K/dc$$

as $c \to 0$, defining the change in lattice parameter $a$, the shear modulus $G$, and the bulk modulus $K$ produced by a solute atom fraction $c$ in the bulk must be known.

The different contributions to the interaction energy with Poisson's ratio $\upsilon$ are:

$$\Delta H_a = \frac{1+\upsilon}{\sqrt{2}\pi(1-\upsilon)} Gb^3 \left(\frac{\mathbf{b}_e}{r}\right) e_a \sin\theta \tag{1a}$$

for the misfit interaction with an edge component $\mathbf{b}_e$ and $\Delta H_e = 0$ for the screw component. For the shear and bulk modulus interaction with the screw components $\mathbf{b}_s$:

$$\Delta H_G = \frac{\sqrt{2}}{16\pi^2} Gb^3 \left(\frac{\mathbf{b}_s}{r}\right) e_G \tag{1b}$$

$$\Delta H_K = 0$$

For the shear and bulk modulus interaction with the edge component $\mathbf{b}_e$

$$\Delta H_G = \frac{\sqrt{2}}{16\pi^2}\left(\frac{1}{1-\upsilon}\right)^2 Gb^3 \left(\frac{\mathbf{b}_e}{r}\right)^2 x$$

$$x e_G[1 - 2/3\sin^2\theta(1 + 2\upsilon - 2\upsilon^2)]$$

$$\Delta H_K = \frac{\sqrt{2}}{16\pi^2}\left(\frac{1}{1-\upsilon}\right)^2 Kb^3 \left(\frac{\mathbf{b}_e}{r}\right) e_K \sin^2\theta \tag{1c}$$

Thus, the total modulus interaction with each component of $b$ is:

$$\Delta H_m = \Delta H_G + \Delta H_K$$

As will be shown later on, the modulus interaction compared with the misfit interaction, is negligible and so it can be omitted.

Consider now the general case in which the dislocation of character $\Phi$ and Burgers vector $\mathbf{b}$ lying on a line $\mathbf{l}$ is dissociated into two partials with Burgers vectors $\mathbf{b}_1$ and $\mathbf{b}_2$ according to Fig. 1. The absolute values of $\mathbf{b}_1$ and $\mathbf{b}_2$ edge components projected on a line perpendicular to $\mathbf{l}$ (where absolute values should be taken) are:

$$b_{e1} = \frac{b}{2}\sec\frac{\pi}{6} \times \sin|\Phi + \pi/6 \tag{2a}$$

and

$$b_{e2} = \frac{b}{2}\sec\frac{\pi}{6} \times \sin|\Phi - \pi/6| \tag{2b}$$

Hence, the maximum misfit interaction energy for the edge component of the leading dislocation $\mathbf{b}_1$ with a solute atom, occuring when $r=b$ and $\theta=-\pi/2$ in Eq. (1a) is:

$$\Delta H_{a1}(\Phi) = -\frac{1}{\pi\sqrt{6}}\frac{(1+\upsilon)}{(1-\upsilon)} e_a G b^3 \times \sin|\Phi + \pi/6| \tag{3a}$$

and for the edge component of the trailing dislocation $\mathbf{b}_2$

$$\Delta H_{a2}(\Phi) = -\frac{1}{\pi\sqrt{6}}\frac{(1+\upsilon)}{(1-\upsilon)} e_a G b^3 \times \sin|\Phi - \pi/6| \tag{3b}$$

It can then be noticed that the binding energies are different for the two partials depending upon the dislocation character. For instance, for a $\Phi=\pi/6$ undissociated dislocation the edge component of the trailing partial vanishes and $\Delta H_{a2}(\pi/6)=0$. Thus, the pinning effect occurs only through the contribution of $\Delta H_m$ which is negligible. It is then expected that for such extended dislocation only the partial $\mathbf{b}_1$ is pinned, with $\mathbf{b}_2$ free to lie under equilibrium conditions at a distance from $\mathbf{b}_1$ where the repulsive force between them balances the attractive one arising from the stacking fault energy determined by its intrinsic value and by the equilibrium amount of Suzuki segregation [14].

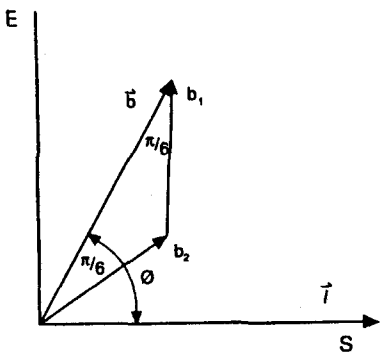


**Fig. 1** Extended dislocation with Burder's vector **b** and character $\Phi$. The two partial components $\mathbf{b}_1$ (leading) and $\mathbf{b}_2$ (trailing) are sown

## *Energetics of segregation*

Having determined the binding energy of a solute atom with each partial, it is necessary to know the equilibrium concentration of solute atoms at dislocations as the second input, in order to assess the energy evolved during the segregation process after it goes to completion. Such concentration can be calculated from the classical treatment of Cottrell and Bilby [18] governed by Boltzmann statistics, and for the case where partials are considered it is:

$$c_{d_1,d_2}(\Phi) = c\,\exp(-\Delta H_{a_1,a_2}(\Phi)/RT) \tag{4a}$$

where subscripts $d_1$, $a_1$ and $d_2$, $a_2$ apply to the leading and trailing dislocation, respectively, $T$ is the equilibrium temperature and $R$ is the gas constant. This approximation was used in previous works [3, 4]. However it has been pointed out that a more proper solute distribution should be governed by Fermi-Dirac statistics [19] to ensure that the atomic solute fraction will nowhere exceed unity. Assuming that the solutes do not interact with each other, the resulting solute distribution is:

$$c_{d_1,d_2}(\Phi) = \frac{c\exp(-\Delta H_{a_1,a_2}(\Phi)/RT)}{1 + c\exp(-\Delta H_{a_1,a_2}(\Phi)/RT)} \tag{4b}$$

and this expression will be used herein. However, notice that $c_{d_1,d_2}$, $(\Phi)$ in the Boltzmann form is recovered when $\Delta H_{a_1,a_2}/RT>1$ and $c\ll 1$ for low concentrations.

If the fraction of solute atoms segregated to the leading dislocation is designated by $f_1$, the number of solute atoms pinned to it divided by the total lattice sites is given by $f_1 c_{d_1}(\Phi)$, while the number of atom sites in that dislocation, divided by the total number of atom sites is $\pi\rho b^2$, $\rho$ being the dislocation density; hence the concentration of solute atoms is $c_{d_1} = f_1 c/\pi\rho b^2$. Similarly, for the trailing partial, $c_{d_2}$ can be written as $c_{d_2} = f_2 c/\pi\rho b^2$ where $f_2$ is the fraction of solute atoms segregated to it. Hence, the evolved heat $\Delta H_d(\Phi)$ of the segregation process due to both partials is:

$$\Delta H_d(\Phi) = f_1 \Delta H_{a_1}(\Phi) + f_2 \Delta H_2(\Phi) \tag{5}$$

Using Eqs (3a) (3b) and (4b), Eq. (5) becomes

$$\Delta H_d(\Phi) = \frac{\pi\rho b^2}{c}\left[\Delta H_{a_1}(\Phi) c_{d_1}(\Phi) + \Delta H_{a_2}(\Phi) c_{d_2}(\Phi)\right] \tag{6}$$

Equation (6) is used to compute the evolved energy as a function of the dislocation character, it is assumed that all dislocations are of the same character $\Phi$. Such situation is generally unrealistic, being observed only in single crystals subjected to flexion [20], where most dislocations are of edge character ($\Phi=\pi/2$), or to torsion [20] where screw dislocations prevail ($\Phi=0$).

### *Influence of dislocation character distributions*

Since $\Delta H_d$ $(\Phi)$ values computed using Eq. (6) indicate the shortcoming of considering all dislocations to be of the same character, possible distributions of $\Phi$ are required in order to compute more realistic values for $\Delta H_d$. Such distribution depends on material internal variables (grain size, stacking fault energy, crystallography etc.) and of the degree and mode of deformation (rolling, drawing, flexion, torsion, etc.), i.e. on experimental mechanical variables. The more experimental information about the dominant dislocation configurations in each case, the more realistic the probability density function ascribed to $\Phi$. The strength of the present approach lies in its capacity to 'average out' much of the underlying com-

plexity of estimating the expected values of $\Delta H_d$. It is worth recalling that many statistically-based models simulating dislocation network evaluation in order to describe mechanical properties are being used at present [21, 22].

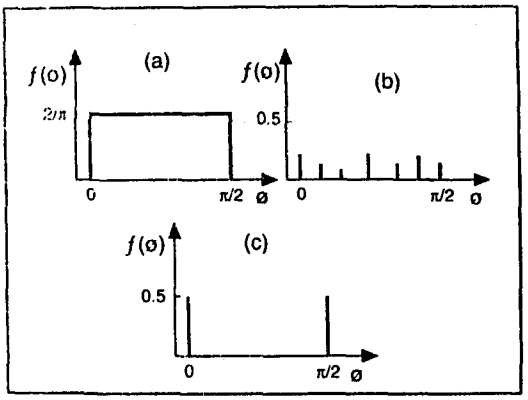


**Fig. 2** Probability density functions of $\Phi$. a) box, b) arbitrary discrete and c) bimodal-extreme-discrete functions

For instance, one can assume that all values of $\Phi$ are equally probable to occur in a heavily deformed alloy, and hence a box distribution as shown in Fig. 2a can be considered. Another situation occurs when only preferred characters are present due to crystallographic constraints and hence only discrete characters are allowed as shown in Fig. 2b. The simplest situation occurs when it is possible to consider that half of the dislocations are screw ones and half are edge ones as shown in Fig. 2c, that gives for $\Delta H_d$ an average between the maximum binding energy $\Delta H_d(\pi/2)$, when edge dislocations are only present, and the minimum binding energy $\Delta H_d(0)$ when only screw dislocations exist.

a) For a box distribution (Fig. 2a) if $f(\Phi)$ is the probability density function of $\Phi$, since $\int_0^{\pi/2} f(\Phi)d(\Phi)=1$, it turns out that $f(\Phi)=2/\pi$. Now if $d\rho=\rho f(\Phi)\, d\Phi$ is the dislocation density having a character between $\Phi-d\Phi/2$ and $\Phi+d\Phi/2$, Eq. (6) becomes

$$\Delta H_d = \frac{2\rho b^2}{c} \int_0^{\pi/2} [\Delta H_{a_1}(\Phi) c_{d_1}(\Phi) + \Delta H_{a_2}(\Phi) c_{d_2}(\Phi)] \tag{7}$$

which is solved numerically. It is worth recalling that this distribution is suitable for deformed alloys when homogeneous arrays of dislocations develop.

b) An arbitrary discrete distribution of dislocations character (Fig. 2b) can be written as

$$f(\Phi) = [\Sigma\, p_i(\Phi_i)]\, [\Sigma\, \delta(\Phi - \Phi_j)]$$

where $p_i(\Phi_i)$ is the fraction of dislocation density with character $\Phi_i$ and $\delta(\Phi-\Phi_i)$ is the Dirac delta function. The product $p_i(\Phi_i)\, \delta(\Phi-\Phi_j)$ exists only if $i=j$, otherwise

if $i \neq j$ then $p_i(\Phi_i\ \delta(\Phi-\Phi_j)=0$. On the other hand $\Sigma p_i=1$. Hence, the evolved heat after the segregation process reaches equilibrium conditions at $T$ is:

$$\Delta H_d = \frac{\pi\rho b^2}{c}\int_0^{\pi/2}\{[\Sigma_i p_i(\Phi_i)]\ [\Sigma_j \delta(\Phi-\Phi_j)]\ [\Delta H_{a_1}(\Phi)c_{d_1}(\Phi) + \\ + \Delta H_{a_2}(\Phi)c_{d_2}(\Phi)]\}d(\Phi) \quad (8)$$

The solution of Eq. (8) is:

$$\Delta H_d = \frac{\pi\rho b^2}{c}\Sigma_i p_i(\Phi_i)[\Delta H_{a_1}(\Phi_i)c_{d_1}(\Phi_i) + \Delta H_{a_2}(\Phi_i)c_{d_2}(\Phi_i)] \quad (9)$$

which is suitable for straight dislocations configurations constrained to glide on specific slip systems.

c) A particular case of the above discrete distributions is the bimodal-extreme-discrete distribution (Fig. 2c) also suitable for straight dislocation arrays where, as said before, half of the dislocations are edge and half are screw. In this case $p_1(0)=1/2$ and $p_2(\pi/2)=1/2$. Applying Eq. (9) yields:

$$\Delta H_d = \frac{\pi\rho b^2}{c}[1/2(\Delta H_{a_1}(0)c_{d_1}(0) + \Delta H_{a_2}(0)c_{d_2}(0)) + \\ + 1/2(\Delta H_{a_1}(\pi/2)c_{d_1}(\pi/2) + \Delta H_{a_2}(\pi/2)c_{d_2}(\pi/2))] \quad (10)$$

As Eqs (3a) and (3b) give $\Delta H_{a_1}(0)=\Delta H_2(0)$, it follows that $c_{d_1}(0)=c_{d_2}=(0)$; also, as $\Delta H_1\ (\pi/2)=\Delta H_2(\pi/2)$ it follows that $c_{d_1}(\pi/2)=c_{d_2}(\pi/2)$ and Eq. (10) becomes

$$\Delta H_2 = \frac{\pi}{c}\rho b^2[\Delta H_{a_e}c_{d_e} + \Delta H_{a_s}c_{d_s}] \quad (11)$$

after making $\Delta H_1(0)=\Delta H_2(0)=\Delta H_{a_s}$, $\Delta H_1(\pi/2)=\Delta H_2(\pi/2)=\Delta H_{a_e}$, $c_{d_1}(0)=c_{d_2}(0)=c_{d_s}$ and $c_{d_1}(\pi/2)=c_{d_2}(\pi/2)=c_{d_e}$. Subscripts ($e$, $s$) refer to (edge, screw) dislocation character. In closing this section it is worth recalling that many other $\Phi$ distributions may be employed in keeping with the specific experimental information available.

### *Dislocation density evaluations*

When estimating $\Delta H_d$ according to the possible probability density functions of $\Phi$, with the aim of comparing its value with the evolved heat compatible with a segregation process for instance when analyzing DSC traces, values of $\rho$ are required. Such values can be determined from the measured release of energy $\Delta H_r$, due to recrystallization in the DSC experiment. The dislocation density $\rho$ is computed from:

$$\rho = \frac{|\Delta H_r|\rho_s}{E_L} \quad (12)$$

where $\rho_s$ is the average density of the material and $E_L$ is the energy of a dislocation per unit length, which was taken as [23]:

$$E_L = \frac{Gb^2}{4\pi A}\left(\ln\frac{r}{r_o}\right) + \frac{Gb^2}{10} \tag{13}$$

where $A=1$ for a screw dislocation and $A=1-\upsilon$ for an edge one while distance $r_o$ is about $b$. For the present computations, $A=0.85$ was adopted. The value of $r$ is generally considered as the mean distance between dislocations, $L_d$, and is related to the dislocation density as follows:

$$L_d = \frac{m}{\rho^{1/2}} \tag{14}$$

where $m$ is a number depending on actual dislocation distribution. In a regular three dimensional array $m$ is in the order of 3, while it is a little higher for a less regular arrangement say $m=5$ [24]. The present work uses $m=4$.

Since Eqs (12), (13) and (14) must be mutually consistent, the following equation allows the iterative computation of $\rho$:

$$\frac{|\Delta H_4|\rho_s}{\rho} = \frac{Gb^2}{4\pi A}\ln\frac{m}{b\rho^{1/2}} + \frac{Gb^2}{10} \tag{15}$$

It should be observed here that other works computing dislocation density from energy measurements and based on specific values for the individual dislocations energy [25, 26], do not involve energy due to interaction and also neglect core energy. Thus, dislocation densities are inversely proportional to the rather arbitrarily assumed value for the energy per unit length of an individual dislocation. Furthermore, the assumptions that no energy due to interactions is involved and that the core energy may be ignored are unlikely, since these factors vary with dislocation density and distribution and hence with the degree of deformation. For the high dislocation densities of the present study, the core energy becomes important. The method presented herein for computing $\rho$ takes duly into account all these facts, making it self-consistent regarding dislocation density, elastic energy per unit of dislocation length, and mean free distance between individual dislocations.

## Numerical results and discussion concerning αCu–Al alloys

In this section the DSC trace features are analyzed in three deformed and non-deformed αCu–Al alloys in connection with the segregation model herein developed. The Cu–Al alloys used here were chemically analyzed and found to contain 3.00±0.04, 6.00±0.07, and 9.0±0.1 wt.% aluminium. They were prepared in a Baltzers VSG 10 vacuum induction furnace from electrolytic copper (99.95 wt.%) and aluminium (99.97 wt.%) in a graphite crucible. The ingots were subsequently hot forged at 923 K to a thickness of 10 mm, pickled to remove oxide from the sur-

face, annealed in a vacuum furnace at 1123 K for 36 h to achieve complete homogeneity, and cooled in the furnace to room temperature. They were then cold rolled to 1.5 mm thickness with intermediate anneals at 873 K, water quenched and finally cold rolled to 0.75 mm thickness (50% reduction). The alloys studied in the nondeformed condition were heat-treated also at 823 K for one hour followed by water quenching in order to start with a material in a highly disordered state which is not expected to disorder substantially after deformation. Hence the DSC trace features can be separated in principle in the deformed and quenched alloys for subsequent comparison. Otherwise, if the alloys were furnace cooled, i.e. highly ordered initially then no DSC heat evolutions due to SRO development could be expected. Also, SRO destruction would be important in the deformed alloys and thus reordering plus other effects occurring simultaneously during a DSC run could not be discriminated directly.

Microcalorimetric analysis of the samples was performed in a DuPont 2000 Thermal Analyzer. Specimen discs of 0.75 mm thickness and 6 mm diameter were prepared and examined for each material condition. Differential scanning calorimetric (DSC) measurements of the heat flow rate were made by operating the calorimeter in the constant heating rate mode (heating rate, 0.333 K $s^{-1}$). Runs were made from room temperature to 740 K. To increase the sensitivity of the measurements, a high purity well-annealed copper disc in which no thermal events occur in the range of temperatures scanned was used as a reference. To minimize oxidation, dried nitrogen ($0.8\times10^{-4}$ $m^3$ $min^{-1}$) was passed through the calorimeter.

### *DSC curves*

Typical traces for the three alloys are shown in Fig. 3 as differential heat capacity *vs.* temperature curves for the 50% cold-rolled condition. They are characterized by three exothermic reactions, namely Stage 1, 2 and 4, and one rather small endothermic reaction designated as Stage 3, all shown in this Figure. The height and area under all these peaks, with the exception of those for peak 3, increase with the aluminium content. Similar traces for quenched specimens of the same alloys quenched from 823 K are shown in Fig. 4; they are somewhat similar to those appearing in Fig. 3 but Stage 4 is absent.

The four Stages observed have been reported in the literature in connection with the following processes:

Stage 1: Short-range-order development assisted by excess vacancies [2, 27–32].

Stage 2: Short-range-order formation in the quenched condition assisted by thermal vacancies [2, 31–33]. In a deformed material, short-range-order and other processes connected with solute segregation to partial dislocations that are the subject of the present study.

Stage 3: Disordering [2, 31, 33].

Stage 4: Recrystallization [2, 34].

The reaction enthalpy for Stage 2 is given in Table 1.

## *Determination of dislocation densities*

This section evaluates dislocation densities in order to compute the extent of segregation of solute atoms to dislocations (next section). To accomplish this, the release of energy due to recrystallization must be known.

The traces in Figs 3 and 4 show that the constant rates at which energy is absorbed after recrystallization in the deformed alloys and after disordering in the quenched material are similar for the same aluminium concentration, being 0.48/0.22/0.05 and 0.52/0.24/0.06 J (mol K)$^{-1}$ for the 19/13/6.5 at.% Al alloys in

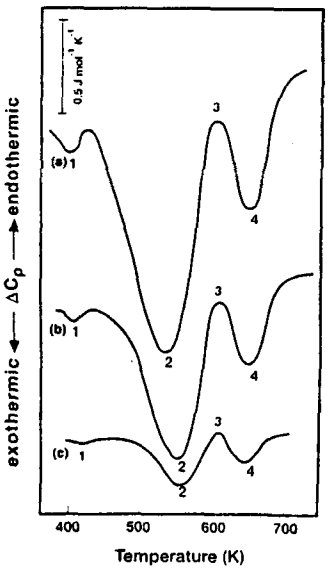


**Fig. 3** DSC traces for 50% cold-rolled alloys at a heating rate of 0.333 K s$^{-1}$. a) Cu-19 at.% Al; b) Cu-13 at.% Al; c) Cu-6.5 at.% Al

**Table 1** Characteristics for stages 1 and 2 in αCu-Al alloys

| Alloy composition At.% | Reaction enthalpy/J mol$^{-1}$ | |
|---|---|---|
| Deformed | $-\Delta H_{1d}$ | $-\Delta H_{2d}$ |
| 19 | 1.8 | 61.9±3.0 |
| 13 | 0.6 | 44.8±2.0 |
| 6.5 | – | 21.2±1.5 |
| Quenched | $-\Delta H_{1d}$ | $-\Delta H_{2d}$ |
| 19 | 11.3 | 28.3±1.8 |
| 13 | 6.9 | 18.9±1.2 |
| 6.5 | 2.3 | 8.9±0.6 |

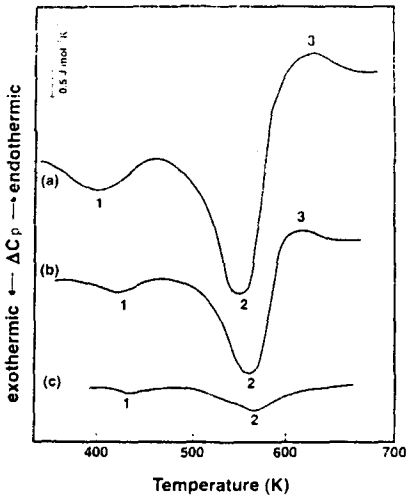


**Fig. 4** DSC traces for quenched alloys at a heating rate of 0.333 K $s^{-1}$. a) Cu-19 at.% Al;. b) Cu-13 at.% Al; c) Cu-6.5 at.% Al

the deformed and quenched conditions, respectively. These results suggest that the deformed specimens are disordering at the rate characterizing the destruction of order at the end of Stage 2 and also that Stages 3 and 4 overlap to some extent, as better seen in Fig. 3c. With the above behaviour, linear substraction of Fig. 4 curves from those in Fig. 3 gives the effective release of energy due to recrystallization, $\Delta H_4$, shown in the curves of Fig. 5, since the overlapping effect or disordering is cancelled. Such energies are listed in Table 2. By solving Eq. (15) iteratively after taking $b=0.26$ nm and $\upsilon=0.3$, values for $\rho$ can be obtained. These values, together with those for $G$ from Hopkin *et al.* [35] are shown in Table 2. It can be seen that the dislocation density increases with the aluminium content. This increase can be readily attributed to the decrease in stacking fault energy as the alloy concentration becomes larger; thus, for the same amount of deformation the recombination or partials is more unlikely, since cross slip is progressively inhibited. For this reason, deformation is absorbed by creating an increasing number of dislocations. Furthermore, the recrystallization temperature increases with aluminium content and the peak becomes broader. These fact may be attributed to the extended nature of dislocations and also to the increasing extent of segregation of solute atoms to the par-

**Table 2** Dislocation density computation (50% cold rolled alloys)

| Alloy composition/ At.% | $-\Delta H_4$/ J $mol^{-1}$ | $\rho_s$ $10^3 \times$kg $m^{-3}$ | Shear modulus GPa | $\rho$ $10^{15}$ $m^{-2}$ |
|---|---|---|---|---|
| 19 | 36.8±1.8 | 8.3 | 46.0 | 4.6 |
| 13 | 28.1±1.5 | 8.5 | 46.7 | 3.8 |
| 6.5 | 12.2±1.0 | 8.7 | 47.6 | 1.2 |

tials with alloy concentration. This process delays the dislocation rearrangement necessary for recrystallization.

### *SRO parameters from DSC traces*

As said above when describing thermal events displayed by DSC traces, Stages 1 and 2 for the quenched alloys have been ascribed to SRO [32], the first one assisted by quenched in vacancies and the second one by thermal vacancies. Such conclusions were drawn from kinetic studies where the equilibrium value of the first SRO parameter at the end of Stage 2 was computed for the studied alloys quenched from 873 K giving thus the values $\alpha_{eq}=-16.4\times10^{-2}/-10.8\times10^{-2}/-5.2\times10^{-2}$ for 19/13/6.5 Al from Fig. 5 in [32]. On the other hand, this parameter may be evaluated from energetic considerations based on the quasi-chemical theory of SRO [36], that is

$$\alpha_{eq} = -\frac{(\Delta H_{1q} + \Delta H_{2q})}{c(1-c)ZW} + \alpha_0 \tag{16}$$

where $Z=12$ is the coordination number, $W=-3.66$ J mol$^{-1}$ [37] is the ordering energy and $\alpha_0$ is the retained first short-range-order parameter after quenching; heats $\Delta H_{1q}+\Delta H_{2q}$ were obtained from Table 1 and $\alpha_0=-14.4\times10^{-2}/-8.9\times10^{-2}/3.64\times10^{-2}$ for 19/13/6.5 Al were also obtained from Fig. 5 of [32]. Thus $\alpha_{eq}=15.9\times10^{-2}\times10^{-2}/10.1\times10^{-2}/4.8\times10^{-2}$ for 19/13/6.5 Al which values, although somewhat lower, are in good agreement with $\alpha_e$ values from kinetic studies. In this way Stages 1 and 2 are unequivocally associated with SRO development, as extensively shown earlier using different experimental and theoretical approaches [2, 27–34].

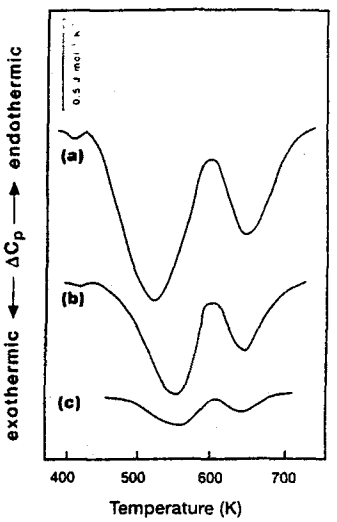


**Fig. 5** Traces resulting from the difference of those corresponding to deformed and to quenched alloys at a heating rate of 0.333 K s$^{-1}$. a) Cu-19 at.% Al; b) Cu-13 at.% Al; c) Cu-6.5 at.% Al

Nevertheless, if the first SRO parameter is computed for the deformed materials by ascribing all the released energy $\Delta H_{1d}+\Delta H_{2d}$ of Stages 1 and 2, to SRO development, then values higher than those corresponding to equilibrium at ending temperatures are obtained. In fact, as release or absorption of energy associated with SRO development or destruction, is proportional to the first SRO parameter variation occurring between the initial and final temperatures of these releases or absorptions [38, 39], thus the equilibrium SRO parameter $\alpha_{ed}$ for deformed alloys after $\Delta H_{1d}+\Delta H_{2d}$ is released can be written as follows, by direct comparison between traces for the materials in both deformed and quenched conditions:

$$\alpha_{ed} = \frac{\Delta H_{1d} + \Delta H_{2d}}{\Delta H_{1q} + \Delta H_{2q}}(\alpha_{eq} - \alpha_o) + \alpha_{od} \tag{17}$$

where $\alpha_{od}$ is the first SRO parameter value after deformation. This comparison. This comparison was preferred instead of using Eq. (16), since Eq. (17) is not dependent on the $W$ value chosen.

Generally, a decrease in SRO is observed after plastic deformation which is caused by the moving dislocations locally destroying order [40–42]. Values of $\alpha_{od}$ after cold-rolling were estimated from [43]:

$$\alpha_{od} = \alpha_o - (\alpha_o - \alpha_m)\,[1 - \exp(-B\varepsilon)] \tag{18}$$

where $\varepsilon$ is the true strain given by $\varepsilon=-\ln(1-R)$ in which $R$ is the degree of cold-rolling reduction (0.5 in this case), $B$ is a parameter lying between 1.0 for no re-ordering and 0.0 for total reordering, and $\alpha_m$ is a limiting value of $\alpha_{od}$ which will be approached asymtotically at larger strains. In the absence of experimental data, $\alpha_m$ can be essentially taken as the equilibrium value of alpha just below the melting temperature, where maximum disorder is achieved. Values for $\alpha_m$ computed using Eqs (9) and (10) of [32], give $-11.9\times10^{-2}/-6.2\times10^{-2}/-3.08\times10^{-2}$ for 19/13/6.5 Al. With all the above data, $\alpha_{od}=-13.7\times10^{-2}/-7.9\times10^{-2}/-3.86\times10^{-2}$ for 19/13/6.5 Al, using $B=1$ which accounts for maximum disorder after the employed degree of cold work reduction. Therefore Eq. (17) yields $\alpha_{ed}=-17.40\times10^{-2}/-11.24\times10^{-2}/-5.75\times10^{-2}$ for 19/13/6.5 Al, which correspond to equilibrium values at 505/505/500 K. These temperatures lie around 80 K below the respective ending temperatures of Stage 2. It is worth noticing that $B=1$ was taken in the computations because deformation was performed at room temperature where partial order restoration is expected to be unimportant, since diffusion is quite limited at this temperature.

In view of the above results, at least another process is occurring during Stage 2 in the controlled alloys. In the deformed material Stage 2 of annealing gives rise to the main increase in yields stress [2]; also there were yield points in single crystals of these alloys [12]. On the basis of the above considerations and of those of other authors [44], the binding of solute atoms to dislocations appears to be the unique contribution to the heat released in Stage 2 in addition to SRO, since no other processes have been experimentally detected up to now.

## *Evaluation of the model*

In this section the energy release due to segregation of solute atoms to dislocations will be evaluated using the model developed herein in order to account for the observed values of the difference $\Delta(\Delta H_2)$ in enthalpy associated with Stage 2, between deformed and quenched materials, for some dislocation character distributions.

In a first step, the binding energies $\Delta H_{ae}$ and $\Delta H_{as}$ between an aluminium atom and the partials of dissociated edge and screw dislocations will be calculated, as extreme values for these energies. For Cu–Al alloys $e_a=0.063$ was computed by using the effective solute radius data of King [45]. The value $e_G=0.28$ was evaluated using Hopkin's data for $G$ [35]. In order to evaluate $e_K$, values for $K$ were first computed from the equation $K=(EG/3)/(3G-E)$ [35] for each alloy composition using also the $E$ data from Hopkin [35] thus obtaining $e_K=0.86$. For a dissociated screw dislocation with a partial edge component $\sqrt{3}b/6$ and a screw component $0.5b$, the largest negative values of misfit interaction energies with an aluminium atom when $r=b$ are $\Delta H_{as}=-0.0084\ Gb^3$ for the 19 at.% Al alloy. For the same alloy and considering a dissociated edge dislocation with a partial edge component $0.5b$ and a screw component $\sqrt{3}b/6$ , $\Delta H_{ae}=-0.0147\ Gb^3$. The total modulus interactions computed are $\Delta H_m=-0.0006\ Gb^3$ for a dissociated screw dislocation and $\Delta H_m=-0.00065\ Gb^3$ for a dissociated edge dislocation. In computing $\Delta H_m$, modulus $K$ was expressed in terms of $G=0.366$ K. Since $\Delta H_m$ is negligible compared with $\Delta H_a$ in both cases, the maximum force between a dislocation and a solute atom is also negligible. Hence, $\Delta H_m$ will be omitted. For a dislocation of character $\Phi$, the calculated variation of $\Delta H_{a_1}$, and $\Delta H_{a_2}$ with $\Phi$ for the leading and trailing partials is shown in Fig. 6. Notice again that $\Delta H_{as}=\Delta H_{a_1}(0)=\Delta H_{a_2}(0)$ and $\Delta H_{ae}=\Delta H_{a_1}(\pi/2)=\Delta H_{a_2}(\pi/2)$. Also, as said before, $\Delta H_2(\pi/6)=0$ and only the leading partial contributes to the pinning effect. Figure 7 shows the calculated curves of evolved heat *vs.* $\Phi$ due to a segregation process, for the three alloys under study, that is when the total population of dislocations is of the same character. It can be noticed that $\Delta H_d$ increases in the same way as the dislocation character, as expected, and it shifts to larger values with higher solute concentrations because of increases in dislocation densities and in the amount of alumimium atoms available for segregation.

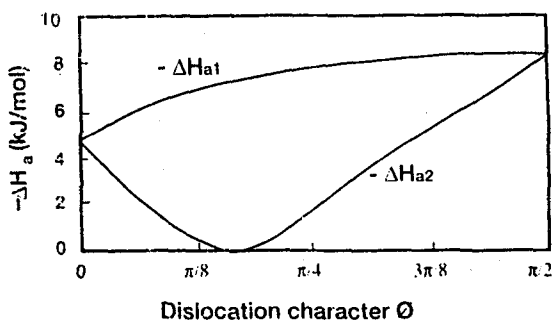


**Fig. 6** Binding energies of a segregated solute atom with a leading ($\Delta H_{a_1}$) or a trailing ($\Delta H_{a_2}$) partial in terms of the undissociated dislocation character $\Phi$

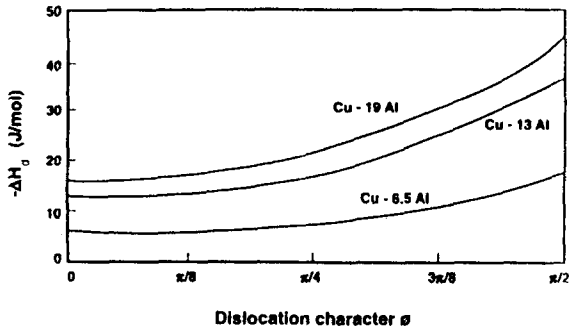


**Fig. 7** Evolved energy associated with the segregation of solute atoms to partial dislocations for 50% cold-rolled alloys as a function of dislocation density character

The second step evaluates the energy released during the pinning process, up to the temperature at which the reaction goes to completion. Comparison of computed values with $\Delta(\Delta H_2)$ measured will allow to decide to what extent the segregation of solute atoms to partial dislocations at the reaction and ($T_f$=580 K) contributes to the energy release observed in Stage 2 for the deformed material. Estimates for $\Delta H_d$ were made considering box distribution shown in Fig. 2a and computed using Eq. (7), arbitrary discrete distribution shown in Fig. 2b calculated using Eq. (9), and bimodal-extreme-discrete distribution shown in Fig. 2c and calculated using Eq. (11). In addition, $\Delta H_d$ was also computed assuming that only edge or screw dislocations are present. Although this situation is unrealistic for this type of deformation, it is considered because it gives the limiting values.

From all dislocation distributions the one giving for $\Delta H_d$ the closet values to $\Delta(\Delta H_2)$ is the bimodal-extreme-discrete distribution. Computation details are shown in Table 3, where ρ values in Table 2 were used.

In order to show the influence of dislocation character distributions on calculated segregation energy, curves of $\Delta H_d$ against alloy composition were drawn as shown in Fig. 8, where the experimentally measured values $\Delta(\Delta H_2)$ were also plotted. The limiting upper and lower values obtained correspond to situations where only edge or screw segments are considered, as said before. All dislocation character distributions here tested give $\Delta H_d$ values below those experimentally obtained. A normal truncated distribution with standard deviation as a parameter was also tested, giving $\Delta H_d$ values between box distribution and those corresponding to a

**Table 3** Results for segregation of solute atoms to dislocations using bimodal-extreme discrete distribution for dislocation density

| Alloy composition/At./% | $-\Delta H_{ae}$/ kJ mol$^{-1}$ | $-\Delta H_{as}$/ kJ mol$^{-1}$ | $c_{de}$ | $c_{ds}$ | $-\Delta H_d$/ J mol$^{-1}$ | $-\Delta(\Delta H_2)$/ J mol$^{-1}$ |
|---|---|---|---|---|---|---|
| 19 | 8.49 | 4.84 | 0.53 | 0.34 | 31.6 | 33.6 |
| 13 | 8.44 | 4.80 | 0.43 | 0.26 | 24.6 | 25.9 |
| 6.5 | 8.38 | 4.77 | 0.27 | 0.15 | 11.7 | 12.3 |

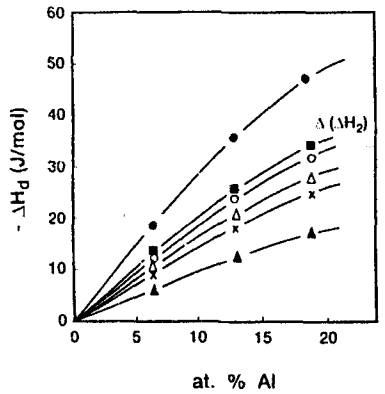


**Fig. 8** Calculated evolved energies associated with the solute segregation process for the indicated probability density functions of $\Phi$ in terms of alloy concentration. Only edge (•) or screw (▲) character is present. Bimodal-extreme-discrete (o), arbitrary discrete (Δ) and box (×) functions. Experimental values (■) are also shown

symmetrical-unimodal-discrete distribution, where the only dislocation character present is $\Phi=\pi/4$. For brevity's sake, these graphs are not shown here.

It can be observed that $\Delta H_d$ values obtained by considering half edge and half screw dislocations are still slightly below $\Delta(\Delta H_2)$ values. One possible explanation for these differences could be that the 50% cold-rolled samples contain more edge than screw dislocations that increase the value of $\Delta H_d$ but no evidence exists for this fact. Also such differences might be attributed to the development of additionally induced short-range-order created around dislocations assisted by the appreciable fraction of solute atoms clustered around them. In any case, without making mean-

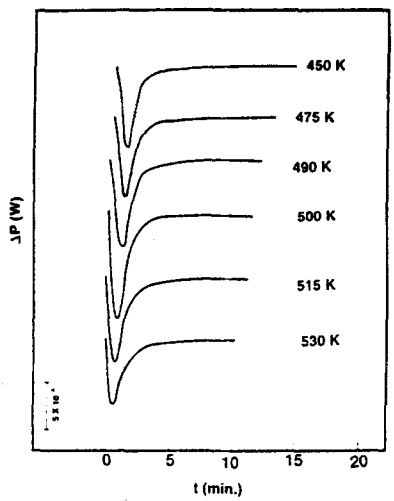


**Fig. 9** Isothermal traces resulting from the difference of those corresponding to deformed and quenched alloys at the indicated temperatures

while any specific decision about the origin of such small differences, the above dislocation character distribution fits quite well with the segregation process, giving an insight into the fine structure of dislocation configurations that cannot be measured in heavily deformed alloys. These last results were also confirmed by isothermal DSC runs. In Fig. 9 the isothermal traces arising from the difference between heats evolved by a deformed and a quenched Cu-19 at.% Al alloy at different temperatures are shown while the experimentally released heats are shown in Fig. 10 for the chosen temperatures. Superimposed on the experimental data, the calculated curve for $\Delta H_d$ using the bimodal-extreme-discrete distribution was also drawn. Good agreement can be seen between both curves, the calculated curve lying slightly below. As the temperature is decreased to about 490 K, the experimental heats depart from the modelled ones and exhibit lower values, as diffusion becomes insufficient for ordering and segregation to attain equilibrium. The energy released during the non-isothermal run in the above alloy is also shown in this plot, thus evidencing fairly good correspondence between experimental and calculated values.

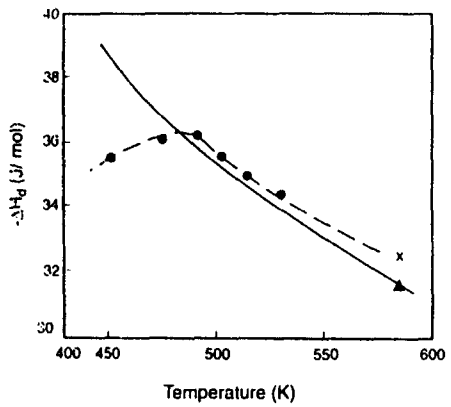


**Fig. 10** Evolved energy associated with the solute segregation process employing the bimodal-extreme-discrete function of Φ. Data points computed from traces of Fig. 9 (•) and the corresponding one from Fig. 5 (×) are shown

In order to study the influence of alloy composition on the calculated values of $\Delta H_d$ using the different dislocation character distributions, a plot of the ratio $\Delta H_d/\Delta(\Delta H_2)$ *vs.* solute concentration was made as shown in Fig. 11. It can be noticed that no matter what distribution is considered, this ratio steadily decreases as the alloy becomes more concentrated. Such results favour the idea that additional dislocation induced SRO accounts for the difference $\Delta(\Delta H_2)$–$\Delta H_d$ obtained for the bimodal-extreme-discrete distribution. The extra SRO formed is further justified because during deformation the alloys become somewhat more disordered than after quenching, due to order destruction produced by cold-work. Thus, during the non-isothermal run, more heat needs to be evolved until the equilibrium degree of order is attained at the ending temperature of Stage 2.

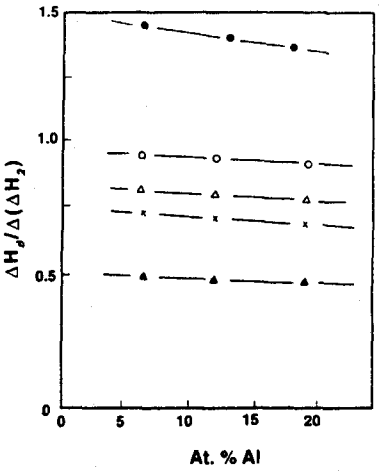


**Fig. 11** Ratio $\Delta H_d/\Delta(\Delta H_2)$ between calculated and experimentally experimentally evolved energy, in terms of alloy concentration for the indicated probability density functions of $\Phi$. Point symbols have the same meaning as in Fig. 8

In the other alloy systems where $\Delta(\Delta H_2)$ values might lie within those of $\Delta H_d$ corresponding to dislocation character distributions that give rise to lower values of released energy, care must be taken in order to univocally decide the proper distribution, since many of them can give $\Delta H_d$ values quite close to one another, introducing a certain lack of predictive capability. Furthermore, for certain distributions, say the normal one, $\Delta H_d$ is influenced by the standard deviation. However, it can be established that the energy evolved during the segregation process gives an indirect insight into the likely dislocation character distribution, which up to now has not been determined experimentally in heavily deformed polycrystalline alloys. As it is well known that low stacking energy alloys exhibiting SRO (such as copper base alloys) develop heavily faulted planar structures composed of straight dislocations when cold-rolled [46, 47], it is concluded that these configurations are constituted by a nearly equal number of edge and screw dislocations. Such distributions were determined in previous works for Cu-20 at.% Mn [3] and Cu-6 at.% Sn [4] suggesting that this is the prevailing distribution for cold-rolled copper alloys. Certainly, as stated before, other deformation modes must influence dislocation character distribution.

## Conclusions

The present study leads to the conclusion that the general model disclosed permitted calculation of the evolved energy associated with solute segregation to partial dislocations during linear heating experiments, thus giving an insight into dislocation character distributions. Application of the model to αCu–Al alloys allows

to infer that when the alloys are cold-worked, segregation of solute atoms to partial dislocations occurs together with short-range-order formation. It is also concluded that half edge and half screw dislocations are present in the deformed alloys. Furthermore it is suggested that dislocation-induced order also is concurrent with the pinning process. When the alloys are quenched, only SRO is developed during the exothermic peak designated as Stage 2 of the anisothermal run.

* * *

The authors would like thank the Fondo de Desarrollo Científico y Tecnológico (FONDECYT) of financial support through Project 1950566, and the Instituto de Investigaciones y Ensayes de Materiales, Facultad de Ciencias Físicas y Matemáticas, Universidad de Chile, for the facilities provided for this research.

## References

1 R. W. Cahn and R. G. Davies, Phil. Mag., 5 (1960) 119.
2 J. M. Popplewell and J. Crane, Metall. Trans., 2 (1971) 3411.
3 A. Varschavsky, Mater. Sci. Eng., 89 (1987) 118.
4 A. Varschavsky, J. Mater. Sci., 26 (1991) 3603.
5 M. Z. Butt and Z. Rafi, J. Mater. Sci. Letts., 10 (1991) 309.
6 A. Varschavsky and E. Donoso, Mater. Sci. Eng., 32 (1978) 65.
7 E. Donoso and A. Varschavsky,Mater. Sci. Eng., 37 (1979) 151.
8 A. Varschavsky and E. Donoso, Mater. Sci. Eng. 40 (1979) 119.
9 S. Fan, K. Inai, S. Onaka and S. Miura, J. Soc. Mater. Sci. Jpn., 41 (1992) 607.
10 A. Varschavsky and E. Donoso, Res Mechanica, 3 (1981) 195.
11 M. Militzer, W. P. Sun and J. J. Jonas, Acta Metall. Mater., 42 (1994) 133.
12 M. Z. Butt, Sci. Int., 2 (1990) 257.
13 F. R. N. Nabarro, Acta Metall. Mater., 38 (1990) 161.
14 A. Varschavsky, Scr. Metall., 9 (1975) 391.
15 D. J. H. Cockayne, M. L. Jenkins and I. L. F. Ray, Phil. Mag., 24 (1983) 1383.
16 J. D. Eshelby, In Physics of Metals, Defects, P. B. Hirsch, ed., University of Cambridge Press, Vol. 2, 1975, p. 1.
17 I. Saxl, Czech J. Phys., 148 (1964) 381.
18 A. H. Cottrell and B. A. Bilby, Proc. Phys. Soc., Lond. A62 (1949) 49.
19 J. P. Hirth and J. Lothe, Theory of Dislocations, 2nd ed., Krieger, Melbourne, F. L., 1991, p. 506 and 512.
20 P. G. Shewmon: Transformations in Metals, 1st. ed. McGraw Hill Book Co., New York, N. Y., 1969, p. 88.
21 L. Shi and D. O. Northwood, J. Mater. Sci., 28 (1983) 5963.
22 R. Bagley, D. I. G. Jones and A. D. Freed, Metall. Trans., 26A (1995) 829.
23 A. Cottrel, An Introduction to Metallurgy, 2nd. ed., Edward Arnold Ltd., London, 1975, p. 334.
24 D. Kuhlmann-Wilsdorf, Trans. TMS-AIME, 224 (1962) 1047.
25 L. M. Clarebrough, M. E. Hargreaves and M. H. Loretto, Proc. Roy. Soc. A., 232 (1955) 252.
26 L. M. Clarebrough, M. E. Hargreaves and M. H. Loretto, Proc. Roy. Soc. B, 257 (1960) 363.
27 M. S. Wechsler and R. H. Kernohan, Acta Metall., 7 (1959) 599.
28 W. Pfeiler, Acta Metall., 36 (1988) 2417.
29 N. P. Kulish and P. V. Petrenko, Phys. Stat. Sol. A., 20 (1990) 315.

30 S. Matsuo and L. M. Clarebrough, Acta Metall., 11 (1963) 1195.
31 A. Varschavsky and M. Pilleux, Mater. Letts, 17 (1993) 364.
32 A. Varschavsky and E. Donoso, Mater. Sci. Eng., A 145 (1991) 95.
33 A. Varschavsky and E. Donoso, Metall. Trans., 15 A (1984) 1999.
34 N. Kuwano, Y. Tomokiyo, C. Knoshita and T. Eguchi, Trans. Jpn. Inst. Met., 15 (1974) 338.
35 M. T. Hopkin, H. Pursey and M. F. Markham, Z. Metallk., 61 (1970) 535.
36 A. Van Den Beukel and S. Radelaar, Acta Metall., 31 (1983) 419.
37 W. Pfeiler and R. Reihsner, Phys. Status Solidi, (I) 97 (1986) 375.
38 N. Kuwano, I. Ogata and T. Eguchi., Trans. Jpn. Inst. Met., 18 (1977) 87.
39 A. Varschavsky, Thermochim. Acta, 203 (1992) 391.
40 J. Olfe and H. Neuhäuser, Phys. Status Solid A, 109 (1988) 149.
41 V. Gerold and H. P. Karnthaler, Acta Metall., 37 (1989) 2177.
42 M. Migschitz, F. Langmayr and W. Pfeiler, Mater. Sci. Eng., A 177 (1994) 217.
43 T. E. Fine and M. E. Nicholson, Scr. Metall., 7 (1973) 383.
44 M. Bader, G. T. Eldis and H. Warlimont, Metall. Trans. A, 7A (1976) 249.
45 H. W. King, J. Mater. Sci., 1 (1966) 79.
46 Y. Tomokiyo, N. Kuwano and T. Eguchi, trans. Jpn. Inst. Met., 16 (1975) 489.
47 A. Varschavsky, E. Donoso and T. Löbel, Proccedings of the Second Interamerican Congress on Electron Microscopy, Cancún, México, 1993, p. 171.